

Using a Digital Camera as a Measuring Device

Salvador Gil,^{1,2} Hernán D. Reisin,² and Eduardo E. Rodríguez^{2,3}

¹ Escuela de Ciencia y Tecnología, Universidad Nacional de San Martín, Provincia de Buenos Aires, Argentina 1653

² Departamento de Física, “J.J. Giambiagi”- Facultad de Ciencias Exactas y Naturales, Universidad de Buenos Aires, Argentina 1428

³ Departamento de Física y Química, Facultad de Ingeniería y Ciencias Exactas y Naturales, Universidad Favaloro, Buenos Aires, Argentina

PACS: 01.50.Lc, 01.50.Pa, 02.40.Hw, 07.05.Fb, 07.05.Hd, 07.07.Hj

We present a set of experiments spanning a broad range of areas of physics that can be carried out using either a digital camera or a web cam. Among them we study the trajectories of water jets, the profile of hanging chains and caustic figures produced by the reflection of light on mirrors of different shapes. This pool of projects shares a common methodological approach and allows for a simple quantitative comparison between theory and experimental results. Since digital cameras are comparatively low-cost laboratory equipment and have become progressively more available, many schools and colleges with limited experimental facilities may benefit from the very cost-effective and challenging projects presented here.

1– Introduction

The main objective of this article is to present and make available a variety of instructive and interesting experiments that can be successfully carried out using low cost equipment: a commercial grade digital camera (or a web cam) with a resolution of 480x640 pixels and a modest home computer. These experimental projects range in terms of theoretical demands, from elementary topics in mechanics or ray theory for light, to more advanced subjects that require some background on solution of differential equations. We begin our study analyzing the trajectory of projectile motion in two dimensions. This first activity is used to illustrate the general technique that is applied later on, to the rest of the projects, i.e. take a photograph of physical phenomena and compare it with the corresponding theoretical expectations. Next we explore the shape of a hanging chain supported by its extremes when it is subjected to different loads. We also apply this technique to study the forms of reflection caustics produced by different types of reflecting mirrors.

Most of these phenomena are not commonly discussed in the introductory textbooks, although they are extremely amenable to undergraduate students. We have adapted them so that they can be easily implemented in a more quantitative manner, using the advantages of digitized images and the same experimental approach. Thus, the procedure serves for any experiment (beyond those presented here) where the relevant physical features are entirely contained in the plane of the photograph. Therefore we believe that this compilation of experiments may be particularly useful to schools and universities with modest experimental facilities.

2– Projectile motion in two dimensions. General procedure.

The purpose of this project is to investigate the trajectory of a water jet steaming out of a hose. A similar study has been performed in the past using a more elaborate experimental arrangement, that required a system to generate drops of water and the use of stroboscopic light.[1] If a nozzle is introduced in the discharge of the hose, with a little practice it is easy to obtain a uniform jet of water. It is important to maintain the flow of water fixed, so that the initial velocity, v_0 , of the jet is also constant. While one student maintains the exit nozzle at a fixed angle, another student takes a picture of the trajectory of the jet.

To obtain a photograph with a minimum of distortion, the camera should be aimed parallel to the normal of the plane that defines the figure of interest. It should be preferentially located along, or close to, the normal passing through the center of the object of interest. To further reduce distortions, it is advisable that the distance of the camera to the object of interest should be much larger than the characteristic dimension of the object. It is also convenient to place vertical and horizontal scales, with easily identifiable marks, close to the water trajectory. In this manner, a single photograph contains all the useful information on the system: initial angle, maximum height, range as well as information on the shape of the trajectory, and the accompanying scales necessary to reconstruct the object of the picture to actual dimensions. For this project we have used a background grid of 20 cm x 20 cm that provides a convenient reference scale. There are several ways to convert the pixel coordinates of the digital photograph into a real spatial coordinate system. Most commercial [1,2,3] and shareware[4] graphic programs (Microsoft® PhotoEditor, Corel Draw®, among others) give the pixel coordinate of the position of the mouse pointer. Another possibility, that we exploited in this project, is to previously trim the digital image to a well-known real size. Then we can create a graph in Excel® with the same dimensions. Importing the trimmed digital image into the plot area of this graph will automatically produce a plot referred to real coordinates. This experimental technique has recently been used by one of the authors to quantitatively study the Bernoulli equation in the drainage of vessels.[5]

If the effect of friction with the air is negligible, the trajectory can be described by the equation of motion of a projectile:

$$y(x) = y_0 + \tan \theta_0 \cdot (x - x_0) - \frac{g}{2v_0^2 \cos^2 \theta_0} \cdot (x - x_0)^2 , \quad (1)$$

where (x_0, y_0) are the coordinates of the exit of the nozzle, θ_0 and v_0 are the initial angle and initial velocity of the jet, and g represents the acceleration of gravity that is antiparallel to the y axis. The range x_{max} and the maximum height y_{max} of the jet are:

$$x_{max} = \frac{v_0^2 \sin(2\theta_0)}{2g} , \quad (2)$$

and

$$y_{max} = \frac{v_0^2 \sin^2 \theta_0}{2g} ; \quad (3)$$

so that

$$\frac{y_{max}}{x_{max}} = \frac{1}{2} \tan \theta_0 , \quad (4)$$

Therefore, the ratio of maximum height to the range, characterize the initial angle of the jet or the projectile. Varying the value of the initial velocity v_0 , it is simple to fit the actual trajectory of the jet with expression (1). In Fig. 1 we present an example of this analysis. In our case, variation of the order of few percent in the value of v_0 , produces noticeable discrepancies between the actual trajectory and the theoretical expectation. Thus the values of v_0 can be determined with an uncertainty of about 4% percent. Near the nozzle we observe a well-conformed jet of water, whereas far from the nozzle, the jet breaks into drops of different sizes. Nonetheless, the jet or the drops follow the same trajectory. This observation may be useful for confronting the students with the Aristotelian misconception that some freshmen students still have, namely that liquid and solids follow different laws of physics.[5]

Furthermore, this value of v_0 can be compared with an independent measurement of the velocity obtained by measurements of the water flux. For this, it is necessary to measure the time it takes the hose to fill a known volume of reference. Since the exit area, A_n , of the nozzle can be measured directly, from the flux of water, $Q = A_n \cdot v_0$, the values of v_0 can be obtained. In our case, the values of v_0 obtained by these two independent methods agree very well within a few percent. Also, it is easy to show that the maximum range is obtained when $\theta_0 = 45^\circ$ in accordance with Eq.(3).

The fact that the observed trajectory and the theoretical expectation, Eq.(1), coincide, indicates that the hypothesis that the effect of friction with the air can be disregarded, is indeed adequate in this case. In all the cases studied we found a very good agreement between the actual trajectory of the jet and the prediction of the model.

We believe this is an instructive project for beginner students, since allow them to verify the usefulness of abstract reasoning to interpret their observations and may be a useful activity to introduce the student to the methodology of science: we elaborate a rational model of reality, make some assumptions, but the final test of our speculation is always the confrontation of the theory with the real data. This activity also illustrates that with a simple experiment, it is possible to explore the theoretical predictions on how a given variable changes as a function of another, in this case, how the range and maximum height vary with the initial angle θ_0 .

3 - Studying catenaries

When traveling along a road, we often notice that the electrical cables hanging between posts and hanging bridges have a characteristic shape. The same applies to chains hanging from their extremes. The curves that hanging chains adopt have intrigued many important scientists in the past. Galileo claimed, erroneously, that this shape was a parabola. It seems that were Leibniz, Huygens, and Johann Bernoulli who solved this problem in response to a challenge made by Jakob Bernoulli in 1691. We call this curve

catenary (from the Latin word for chain). Its solution can be found in many textbooks. In Appendix A, we reproduce a simple justification highlighting basic physics ideas used in its derivation.

For a chain of length L_c with uniform mass density, hanging from two points located at the same height h , relative to its vertex and separated by a distance L in a uniform gravitational field, the expression of the catenary is:

$$y(x) = \frac{1}{\lambda} \cdot (\cosh(\lambda \cdot x) - 1), \quad (5)$$

where λ can be found solving the equation:

$$\frac{\lambda \cdot L_c}{2 \cdot (\lambda \cdot h + 1)} = \tanh(\lambda \cdot L/2). \quad (6)$$

In Fig. 2 we show the digital image of a chain. Overlapped on this image we also see the shape of the catenary obtained using Eqs.(5) and (6). For comparison, in this figure we also see the shape of the parabola that has the same vertex and the same hanging points. The catenary clearly gives a much better description of the actual shape.

In Fig. 3 we show the image of a uniformly loaded chain. Here the loads (150g each) were uniformly distributed horizontally on a 125 g chain, so that $\rho(x) \cdot ds/dx \approx \text{constant}$. Overlapped on this image we also show the shape of the catenary and a parabola. In this case the parabola gives a better description of the shape of the chain, in agreement with the theoretical expectation (see Appendix A). This situation can also be tested in actual hanging bridges.[6] This experimental approach can also be used to test the theoretical expectation of the shape for nonuniform cables.[7]

It is interesting to note that the forces along the hanging chain (loaded or unloaded) are pure tensile forces, as due to its flexibility the chain cannot support any compression. Therefore, if the system were flipped, all the forces due to weight are reversed and the curve along the chain is subject to pure compression forces. Since many traditional construction materials, such as bricks and stone, can withstand great compression but small tensile forces, the catenary would make a perfect arch using these types of materials. The same idea can be used for designing a loaded arch. We charge the chain with the required load and observe the shape it takes. By flipping the figure we obtain the form of the arch that is subject to pure compression consistent with that load. The famous Catalan architect Antoni Gaudi used this principle to design some of the beautiful and astonishing structures he built in Barcelona.

4– Studying reflection caustics

When observe a filled cup of white tee or coffee, we often see a heart-like figure, particularly if there is a single light source in the room, shining laterally to the cup. This same figure can be observed inside a gold ring [8,9] when it is illuminated laterally. These figures are examples of the caustic figures, produced by the envelope of the reflected rays (known as catacaustic) onto the circular surface of the cup or the ring, as

Fig. 4 schematically illustrates. Many great mathematician and physicists have worked on this interesting problem, among others: C. Huygens (1629-1695) and J. Bernoulli (1667-1748). [10,11]

In general, it is possible to find the form of the caustic for any type of reflecting curve. If the form of the concave reflecting surface is given by $y = f(x)$, it can be shown that the parametric equations for the caustics, produced by a light source located at $x \rightarrow -\infty$, are [12] (see Appendix B):

$$\begin{cases} y_c(t) = f(t) + \frac{(f'(t))^2}{f''(t)}, \\ x_c(t) = t + \frac{f'(t) \cdot [1 - (f'(t))^2]}{2f''(t)} \end{cases} \quad (7)$$

For our experiment we plotted the profiles of different mirrors in a one-to-one scale. We glued this plot to a piece of expanded polycarbonate slab, 2 cm thick. Then we carefully cut the silhouette of the curve out of the plate, with a thin hot wire (heated by an electrical current) using the plot as reference route. A strip of aluminized Mylar, about 2 cm wide and 20 μm thick was glued onto the wall. Fig. 5 illustrates the procedure used for fabricating mirrors with predefined shapes.

In Fig. 6 we show the image of a circular mirror illuminated from the left. The image of the caustic is very clear. Overlapped on this image we have included the curve that describes the shape of the mirror and its corresponding caustic according to Eqs. (7). We found that using the Sun as the light source produced the best results. The agreement between the theory and observation is very good. In Fig. 7 we present the results for the case of an exponential mirror and its caustic.

5– Other projects using a digital camera

There are a number of other experiments that can profit from the advantages of a digital image for a quantitative analysis and comparison against theory. For example, most beginner students are familiar with nodes and antinodes in a vibrating string. The generalization of this idea to the vibration of a two-dimensional plate is relatively simple, where instead of nodes (points) we find nodal curves. Spreading white sand on a vibrating plate can easily reveal these shapes. Sand accumulate along the nodal lines known as Chladni figures, produced at different resonance frequencies. [13,14] If we take a digital photograph of the patterns produced at each resonant frequency, it is possible to compare the experimental figures with the predictions of the model.

Other simple and interesting project consists in studying the shape of shadows cast by a lampshade on the wall. Recently, K. E. Horst [15] has discussed this problem using a visual method to characterize the shape of the shadow, its implementation using digital camera is very straight forward.

The lateral deflection of a beam is classical problem that attracted the interest of great scientists in the past. [16] The case of small and large [17] transverse deflections of a

horizontal beam, fixed at one end and subject to varying loading is discussed in many textbooks on elasticity. In both cases, the digital photograph has the advantage of acquiring a great amount of information on the system in a single shot. Therefore it is possible to compare the shape of the beam for different loading, with the theoretical predictions.[17]

7– Summary and conclusions

We have examined the advantages of using a digital camera for carrying out several quantitative experiments. Since the digital cameras are becoming increasingly available at discount prices, and all the materials used in these projects can be found in any hardware shop at very low costs, we hope that these projects can be implemented with no difficulty at almost any school or college.

The experiments proposed here call attention on interesting phenomena in different areas of physics that are challenging, instructive, and not usually covered in regular courses of introductory physics. In all cases the observation can be quantitatively confronted with the corresponding theory, and from this comparison it is possible not only to test the theory, but also to obtain useful information from the system. For example in the study of the trajectory of the water jet we found that: a) the hypothesis proposed with in regard to the small effect of the air friction is indeed adequate, and b) the parameters characterizing the emerging jet (i.e. initial velocity, initial angle, range and maximum height) can be readily obtained from the fit of the theory to the observed trajectory. This activity may be useful for demonstrating that liquid and solids follow same laws of physics.

The study of the shapes of loaded and unloaded chains provide an instructive insight into the shape of hanging cables and hanging bridges. Furthermore, the study of the caustic figures gives a quantitative view of a classical phenomenon, often observed in coffee cups and gold rings.

Finally, the methodological approach used in these projects, clearly illustrates the basic ideas of the scientific method. Given a problem, we search for a rational explanation based upon the accepted paradigms. Then, we must always test the results of our theoretical predictions against the actual observations to accept or reject our theories.

Appendix A

Catenary

We briefly review the physical assumptions that lead to the equation of the catenary. Consider a chain of length L_c and mass M_c suspended by its extremes as indicated in Fig. 8. The weight of an infinitesimal element of length ds in a uniform gravitational field is: $dP = \rho(x).g.ds$, where g is the value of the acceleration of gravity and $\rho(x)$ is the local mass density per unit of length of the chain. If $H(x)$ and $V(x)$ are the horizontal and vertical components of the tension of the chain at the point of coordinate x , the equilibration of the forces along the x and y axes leads to:

$$H(x + dx) = H(x) = H_0 \quad (A1)$$

and

$$V(x + dx) - V(x) = dV = dP = \rho(x) \cdot g \cdot ds, \quad (A2)$$

where H_0 represents the tension of the chain at the vertex (where $dy/dx=0$). The tension of the chain at the point of coordinate x , is tangent to the curve $y(x)$, thus:

$$\frac{V(x)}{H(x)} = \frac{dy}{dx}. \quad (A3)$$

This relation is based on the physical condition that the chain is subject only to tensile forces.

Differentiating (A3) and combining it with (A1) and (A2), we obtain:

$$dV = \frac{d^2y}{dx^2} \cdot H_0 \cdot dx = \rho(x) \cdot g \cdot ds. \quad (A4)$$

Note that if $\rho(x) \cdot ds/dx = \text{constant}$, then it follows immediately that the shape of the chain $y(x)$ is a pure parabola. This situation will be the case, if on a chain of negligible weight, we hang masses that are uniformly distributed horizontally: as in the example shown in Fig.(5) or in hanging bridges, where most of the weight is on the platform of the bridge. Yet in general, no such particular condition occurs and (A4) must be solved explicitly for each function $\rho(x)$.

Since $ds = dx \cdot \sqrt{1 + (dy/dx)^2}$, we can write (A4) as:

$$\frac{d^2y}{dx^2} = \lambda(x) \cdot \sqrt{1 + \left(\frac{dy}{dx}\right)^2}, \quad (A5)$$

where: $\lambda(x) = \rho(x) \cdot g / H_0$. Equation (A5) can be integrated by substituting $z(x) = dy/dx$:

$$\int \frac{dz}{\sqrt{1+z^2}} = \int \lambda(x') \cdot dx' \Rightarrow z = \frac{dy}{dx} \Big|_x = \sinh(u(x)) + c_1, \quad (A6)$$

where $u(x) \equiv \int \lambda(x') \cdot dx'$. In consequence, the form of the chain for an arbitrary mass

distribution must be solved numerically for each particular case.[7] For the case of constant mass density $\rho(x) = M_c/L_c$, $\lambda = M_c \cdot g / (H_0 \cdot L_c)$ is a constant, and then expression (A6) reduces to: $dy/dx = \sinh(\lambda \cdot x) + c_1$. If we choose the origin of coordinates to coincide with the vertex of the chain (where $dy/dx=0$) then $c_1=0$. Integrating (A6) yields

$y(x) = \frac{1}{\lambda} \cosh(\lambda \cdot x) + c$. Using the condition $y(x=0)=0$ leads to:

$$y(x) = \frac{1}{\lambda} \cdot (\cosh(\lambda \cdot x) - 1). \quad (A7)$$

The constant λ can be obtained from the boundary conditions, namely position of the extremes and the length of the chain L_c . If the hanging extremes are at the same height h , and separated by a distance L . From (A7) we have:

$$h = \frac{1}{\lambda} \cdot (\cosh(\lambda \cdot L/2) - 1). \quad (A8)$$

The length of the chain is:

$$L_C = 2 \cdot \int_0^{L/2} \sqrt{1 + (dy/dx)^2} \cdot dx = \frac{2}{\lambda} \cdot \sinh(\lambda \cdot L/2). \quad (\text{A9})$$

Combining (A8) and (A9) gives:

$$\frac{\lambda \cdot L_c}{2 \cdot (\lambda \cdot h + 1)} = \tanh(\lambda \cdot L/2). \quad (\text{A10})$$

Which relates the parameters: λ , L , L_c , and h .

Appendix B Caustic

The phenomenon of the caustic can be understood using the laws of geometrical optics. The caustic can be defined as the envelope of a family of rays transmitted (diacaustic) by a lens or reflected (catacaustic) by a mirror. In order to make this article self contained, in this appendix we briefly summarize the theoretical connection between the shape of the caustic and the reflecting surface. There are several ways to obtain the equations of the caustic of a mirror.[8,9,10] In this appendix we summarize the argument originally discussed in Ref.[12], based on the Legendre transformation.[18, 19]

Geometrically, there are two equivalent manners to represent a locus. By means of the conventional point geometry, the curve is characterized by the relation $y=g(x)$. Equivalently, a family of tangents to the curve can characterize the same locus (see Fig. 9). Since each straight line can be described by its slope $p(=dg(x)/dx)$ and the intersection with the y axis (ψ), the relation $\psi=\psi(p)$ can be used to represent a family of tangent to the curve. This last representation is known as the Plücker line geometry.[19] It can be shown that $y=g(x)$ and $\psi=\psi(p)$ are two equivalent representations of the locus.[19]

From the left panel of Fig. 9, it follows that:

$$p = \frac{(y_0 - \psi)}{x_0}, \text{ or } \psi = y_0 - p \cdot x_0 \quad (\text{B1})$$

Therefore, if we know the family of tangents expressed by $\psi=\psi(p)$, according to (B1) $\partial\psi/\partial p = -x$. The conventional point representation, $y=g(x)$, can obtain from Eq.(B1):

$$y = g(x) = x \cdot p + \psi(p), \quad (\text{B2})$$

This type of transformations is often used in analytical mechanics when one wants to go from the Lagrangean formulation of a problem to a Hamiltonian one. Also, in thermodynamics these transformations are very useful to transform the thermodynamic potentials from one representation to another, i.e. from the Enthalpy representation to the Helmholtz free energy representation.

Consider a concave reflecting surface characterized by $y=f(x)$ and a beam of horizontal parallel rays incident from the left. Fig. 10 schematically illustrates this situation. If θ is the angle of incidence on the mirror, relative to the normal to the reflecting surface, then $\tan \theta = -1/f'(x)$. The slope of the reflected ray is: $p=\tan(2\theta)$ and its intersection with the y -axis is ψ . The equation of the reflected ray can be written as:

$$Y - f(x) = p(X - x), \quad (\text{B3})$$

where

$$p = \tan(2\theta) = 2f'(x)/(1 - (f'(x))^2), \quad (\text{B4})$$

Y and X are the coordinates of any point on the reflected ray and $(x, f(x))$ is the point of incidence of the incoming ray on the mirror. Accordingly we can write:

$$\psi(p) = Y(X = 0) = f(x) - x \cdot p. \quad (\text{B5})$$

This last equation can be regarded as the expression of the family of tangent lines that characterize the locus of the caustics in Plücker line geometry.[12,19] In order to convert to the conventional point geometry of the caustic, $y_c=g(x_c)$, we can use the Legendre transformation:

$$x_c = -d\psi / dp = (p - f'(x)) \frac{dx}{dp} + x. \quad (\text{B6})$$

Combining Eqs.(B4) and (B6) we have:

$$x_c = \frac{f'(x) \cdot [1 - (f'(x))^2]}{2f''(x)} + x. \quad (\text{B7})$$

From Fig. 10, we can write:

$$y_c = x_c p + \psi(x). \quad (\text{B8})$$

Replacing Eqs.(B4), (B5) and (B7) in this last expression we have:

$$y_c = \frac{(f'(x))^2}{f''(x)} + f(x). \quad (\text{B9})$$

Therefore the parametric Equations of the caustics are:

$$\begin{aligned} y_c(x) &= f(x) + \frac{(f'(x))^2}{f''(x)}, \\ x_c(x) &= x + \frac{f'(x) \cdot [1 - (f'(x))^2]}{2f''(x)} \end{aligned} \quad (\text{B10})$$

Figure captions

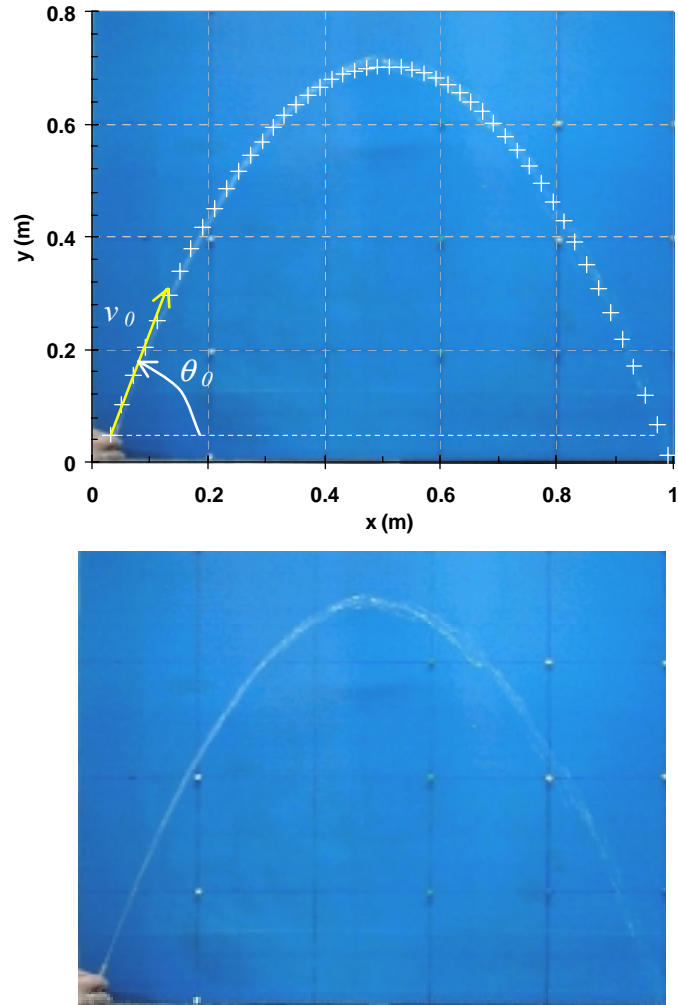


Fig. 1. Trajectory of a water jet. In the upper panel, we see the digital image superposed with the theoretical expectation for this trajectory according to Eq.(1), represented by crosses. The parameters v_0 and θ_0 , can be obtained from the fit to the actual trajectory. In the lower panel we see the plain photograph of the jet.

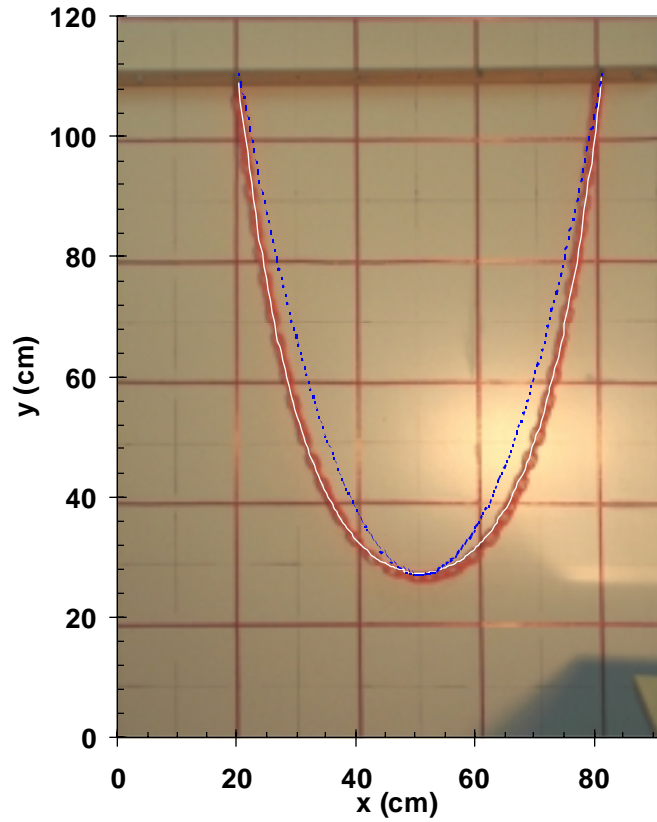


Fig. 2. Superposition of the image of a ganging chain and the theoretical expectation (heavy continuous line) given by Eqs.(5) and (6). For reference, in dashed lines, we show the parabola that goes through the vertex and hanging points. The difference is very clear. The catenary describes the shape of the chain more precisely.

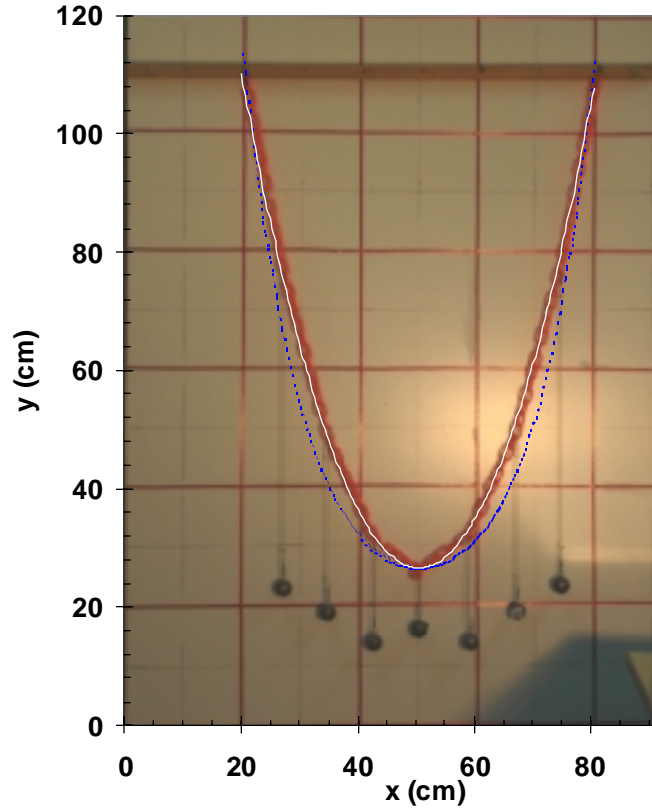


Fig. 3. Image of a uniformly loaded chain. The heavy line is a parabola and the dashed line is a catenary. The parabola gives a better description of the shape of the chain, in consonance with the theoretical expectation.

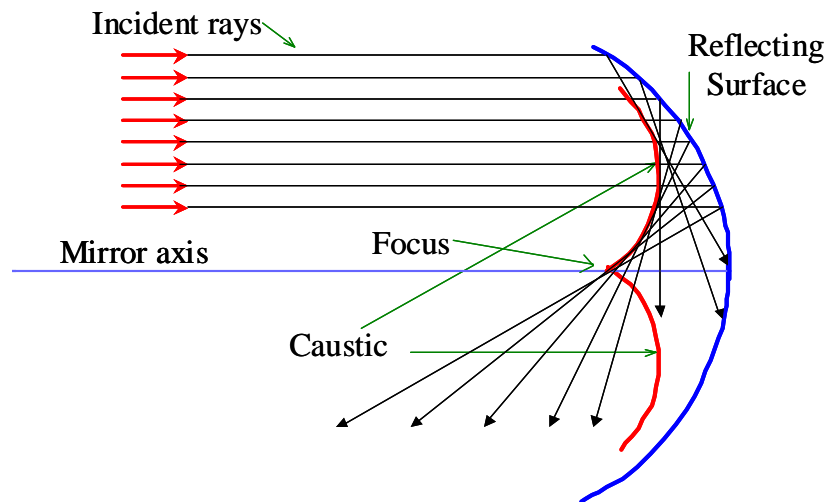


Fig. 4. Schematic diagram of the formation of the caustic (catacaustic). The envelope of the reflected rays is known as the caustic of the reflecting surface. Note that the region enclosed between the caustic and the reflecting surface will present an enhancement in illumination, as a result of the superposition of incident and reflected rays that pass through this space.

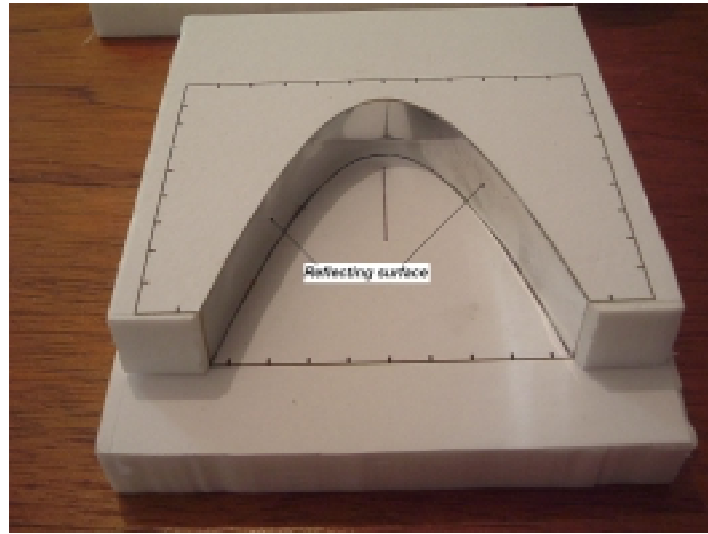


Fig. 5. Schematic diagram of the experimental arrangement for building a mirror with a predefined shape.

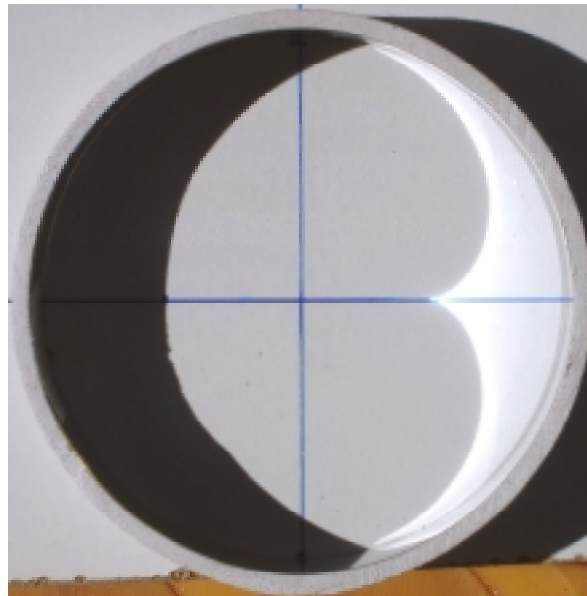
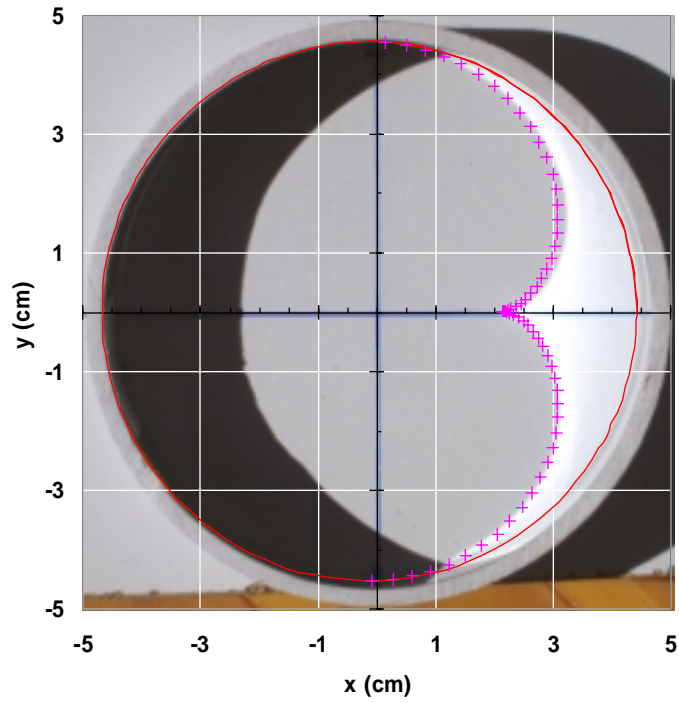


Fig. 6. Superposition of the caustic for a circular mirror (catacaustic) and the theoretical expectation given by Eq.(7). The lower panel is a photograph of the phenomenon.

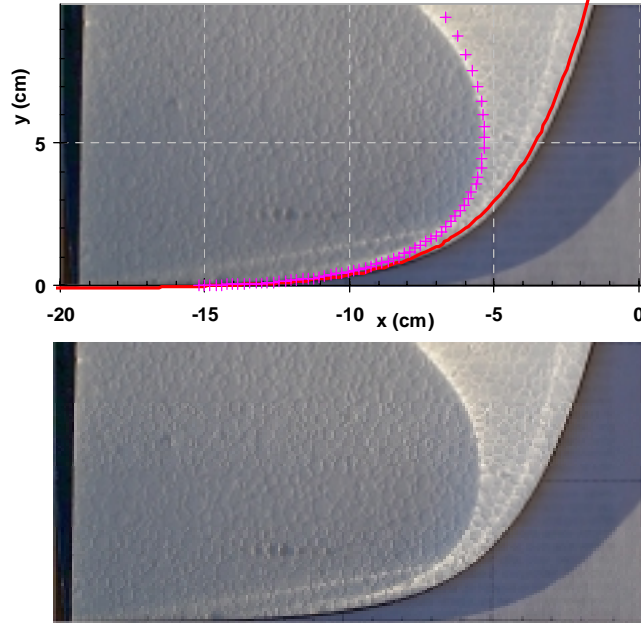


Fig. 7. Superposition of the caustic for an exponential mirror and the theoretical expectation given by Eq.(7). The lower panel is a photograph of the phenomenon.

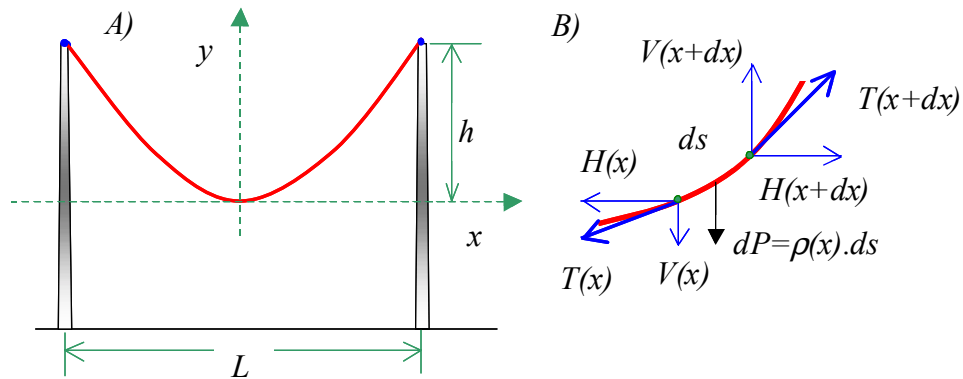


Fig. 8. A) Chain or flexible rope or chain suspended by its extremes. The coordinates of the hanging points are $(-L_2, h)$ y (L_1, h) , with $L_1 + L_2 = L$. B) Forces that act on an infinitesimal element of chain of length ds .

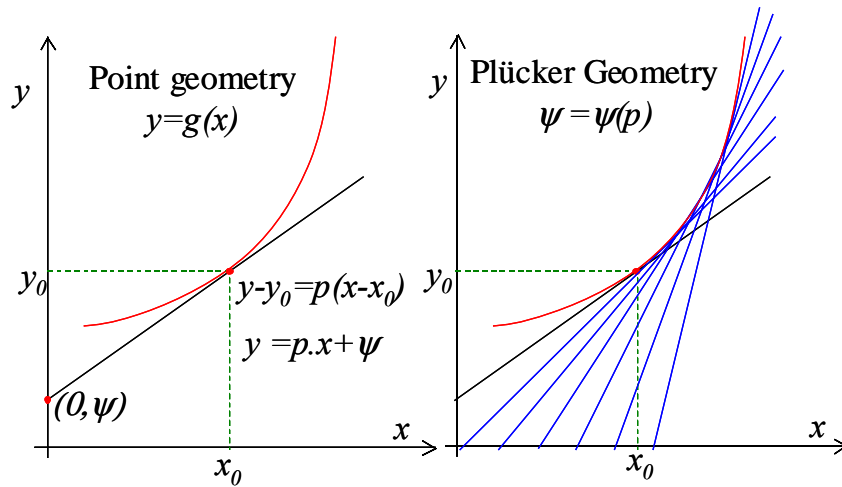


Fig. 9. There are two equivalent forms to represent a curve. By the conventional point geometry, the curve is characterized by the relation $y=g(x)$. Equivalently, the same locus can be characterized by a set of tangent lines to the curve determined by the relation $\psi = \psi(p)$. The connection between these two representations is expressed by the Legendre transformation.

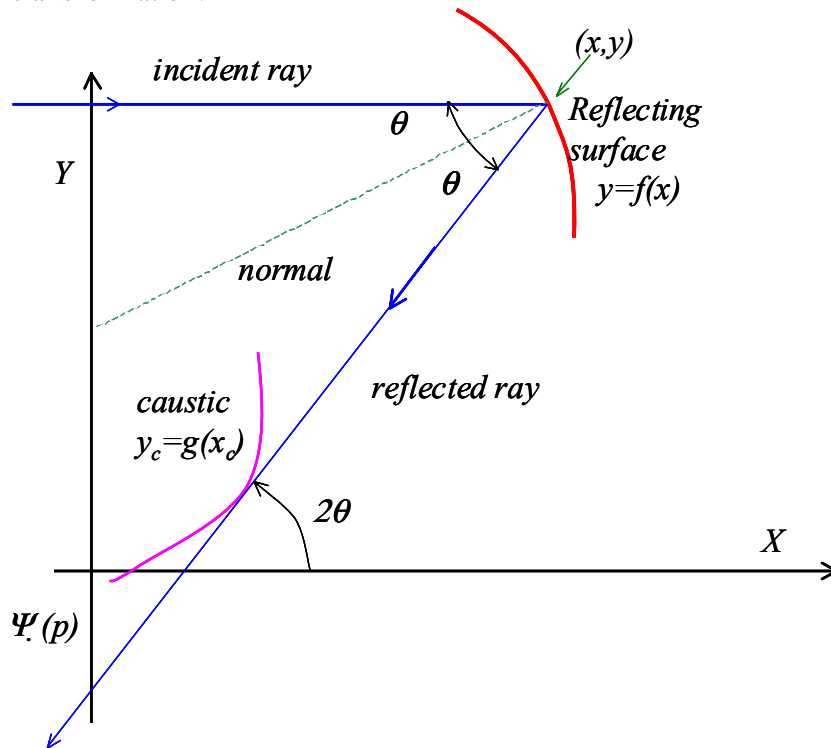


Fig. 10. Schematic diagram of the relation between the reflecting surface, represented by $y=f(x)$ and the caustic characterized by $y_c(x_c)$. The incident rays originate from a source on the far left.

-
- ¹ Logger Pro 3 – Vernier software www.vernier.com
- ² VideoPoint Capture II – www.Pasco.com
- ³ A. Heck. Coach: an environment where mathematics meets science and technology. In: Proceedings ICTMT4, Plymouth, 1999, W. Maull & J. Sharp (eds.). CD-ROM published by the Univ. of Plymouth, UK, 2000.
- ⁴ xyExtract Graph Digitizer, <http://www.gold-software.com/download5149.html>
- ⁵ M. E. Saleta, D. Tobia, and S. Gil, “Experimental study of Bernoulli's equation with losses,” *Am. J. Phys.* **73**, (7) 598-602 (2005).
- ⁶ Qualitative displays of these phenomena are shown in some science museums, for example MateUBA- Buenos Aires: <http://www.fcen.uba.ar/museomat/mateuba.htm>
- ⁷ M.C. Fallis, “Hanging shapes of nonuniform cables,” *Am. J. Phys.* **65**, (2)117-122 (1997)
- ⁸ Ch. Ucke and C. Engelhardt, “Playing with caustic phenomena,” published in the proceedings of the GIREP/ICPE conference “New ways in physics teaching”, Ljubljana, August 21 to 27, pages 440-444 (1996).
- ⁹ A.D. McIntosh, “An equation for the caustic curve,” *Phys. Educ.* **25**, 171-173 (1990).
- ¹⁰ Famous Curves Index, Turnbull Www Server, School of Mathematical and Computational Sciences, University of St Andrews, UK. <http://turnbull.mcs.st-and.ac.uk/history/Curves/Curves.html>.
- ¹¹ Eric W. Weisstein World of Mathematics 1999 CRC Press LLC, 1999 Wolfram Research, Inc. <http://mathworld.wolfram.com/topics/CausticCurves.html>
Eric W. Weisstein. "Caustic." From *MathWorld*--A Wolfram Web Resource. <http://mathworld.wolfram.com/Caustic.html>
- ¹² C. Bellver-Cebreros and M. Rodriguez-Danta “Caustics and the Legendre transform,” *Optics Communications*, **92**,187– 192 (1992)
- ¹³ J. R. Comer, M. J. Shepard, P. N. Henriksen, and R. D. Ramsier, “Chladni plates revisited,” *Am. J. Phys.* **72**, (10)1345-1346 (2004)
- ¹⁴ T. D. Rossing, “Comment on "Chladni plates revisited," by J. R. Comer, M. J. Shepard, P. N. Henriksen, and R. D. Ramsier [*Am. J. Phys.* **72** (10), 1345-1346 (2004)],” *Am. J. Phys.* **73**, (3)283- (2005)
- ¹⁵ K.E. Horst, ”The Shape of Lamp Shade Shadows,” *Phys. Teach.* **39**, 139-140 (2001)
- ¹⁶ Th. Hopfl, D. Sander, and J. Kirshner., “*Demonstration of different bending profiles of a cantilever caused by a torque or a force*” *Am. J. Phys.* **68**, 1113 -1115 (2001).
- ¹⁷ A. Valiente, “An experiment in nonlinear beam theory” *Am. J. Phys.* **72**, (8)1008 - 1012 (2004).
- ¹⁸ H. Goldstein, C. Poole, and J. Safko, *Classical Mechanics*. Addison-Wesley, Boston, MA, 3rd ed. .2001.
- ¹⁹ H. Callen. *Thermodynamics and an Introduction to Thermostatistics*. John Wiley and Sons, 2nd edition, 1985.